Computers & Geosciences 106 (2017) 209–216

Contents lists available at ScienceDirect

Computers & Geosciences

journal homepage: www.elsevier.com/locate/cageo

Research paper

# Automatic fracture detection based on Terrestrial Laser Scanning data: A new method and case study

Ting Cao[a,b], Ancheng Xiao[a,b,*], Lei Wu[a,b], Liguang Mao[c]

[a] School of Earth Sciences, Zhejiang University, Hangzhou, Zhejiang 310027, China
[b] Research Center for Structures in Oil & Gas Bearing Basins, Ministry of Education, Hangzhou, Zhejiang 310027, China
[c] College of Geoscience and Surveying Engineering, China University of Mining and Technology, Beijing 100083, China

ARTICLE INFO

*Keywords:*
LiDAR data
3D geometry
Fracture identification
Surface density

ABSTRACT

Terrestrial Laser Scanning (TLS), widely known as light detection and ranging (LiDAR) technology, is increasingly used to obtain rapidly three-dimensional (3-D) geometry or highly detailed digital terrain models with millimetric point precision and accuracy. In this contribution, we proposed a simple and unbiased approach to identify fractures directly from 3-D surface model of natural outcrops generated from TLS data and thus acquire surface density, which can provide important supplement data for fracture related research. One outcrop from the Shizigou anticline in the Qaidam Basin (NW China) is taken as the case to validate the method and obtain optimal parameters, according to the references of surface density measured in the field and from the photos taken by high-resolution camera. The results show that with suitable parameters, the proposed method can identify most structural fractures quickly, providing a solution of extracting structural fractures from virtual outcrops based on TLS data. Furthermore, it will help a lot in analyzing the development of fractures and other related fields.

## 1. Introduction

Fractures widely develop in rocks of various lithologies and are important for understanding the deformation mechanism (e.g., stress-strain property) in a specific area (Olson et al., 2009; Strijker et al., 2013; Zeng et al., 2012a). They reduce the rock strength by breaking the internal coherency, inducing geological hazards (e.g., landslides and debris flow) and increasing risk of collapse of buildings on the rock. On the other hand, however, they can form good reservoirs in tight sandstones, such as the Paleogene Ganchaigou Formation in the Qaidam Basin of western China (Feng et al., 2013; Li and Wang, 2001), and therefore play a significant role in oil & gas exploration (Gale et al., 2007; Olson et al., 2009). Recent studies of fractures are generally based on direct measurements in the field (Awdal et al., 2016; Watkins et al., 2015; Su et al., 2014), analysis of borehole loggings (Lacazette, 2009; Prioul and Jocker, 2009) and signal processing of high-resolution seismic data (Hart, 2006; Lohr et al., 2008; Masaferro et al., 2003). Among them, field measurement is the most prevalent way of high precision and accuracy, but usually time-consuming, dangerous and limited by reach of measurement. A new way of extracting fracture-related information (e.g., fracture geometries, surface density) efficiently, safely and precisely is quite necessary. Currently, non-contact measuring techniques, such as photogrammetry and LiDAR (Light Detection and Ranging), provide alternative approaches to in-situ measurement of fractures from high resolution images and 3-D point clouds of rock mass exposures.

The two-dimensional (2-D) image detection method (photogrammetry) extracts fractures according to changes of pixel intensities, and can be implemented both manually and automatically. Image auto-detection based on edge detection algorithms (Bao et al., 2015; Canny, 1986; Lopez-Molina et al., 2013; Sun et al., 2016) is faster and more objective than the manual one. Whilst, it is influenced largely by quality of the images (e.g., resolution, exposure, light condition), and the results usually contain much meaningless information (Ferrero et al., 2009). Image-based fracture identification, both manually and automatically, faces a nearly insurmountable problem of how to extract convincing information of fractures, which are 3-D in nature, from 2-D photos.

The Terrestrial Laser Scanning (TLS), an emerging LiDAR technology that provides high-resolution 3-D topography (millimetre accuracy) and color images of field outcrops, has been gradually changing the situation (Buckley et al., 2006, 2008) in recent years. Terrestrial Laser Scanners are now small enough to be taken to the field even in tough geographic conditions, and able to capture outcrops (including

* Corresponding author at: School of Earth Sciences, Zhejiang University, Hangzhou, Zhejiang 310027, China.
*E-mail address:* xiaoanch@zju.edu.cn (A. Xiao).

http://dx.doi.org/10.1016/j.cageo.2017.04.003
Received 6 January 2016; Received in revised form 28 February 2017; Accepted 4 April 2017
Available online 06 April 2017
0098-3004/ 

topography and surface color) with high accuracy. Because of these advantages, a growing number of applications has been put forward in various fields, including engineering construction (Wang et al., 2014), agriculture and forestry managements (Liang et al., 2016; Ouédraogo et al., 2014), monitoring of topography and channels (Goodwin et al., 2016; Kuo et al., 2015) and particularly rock surface information extraction (Ahlgren and Holmlund, 2003; Hodgetts, 2013; Slob et al., 2002; Sturzenegger and Stead, 2009). Two kinds of approaches were proposed to detect fractures using 3-D TLS surface data, based on intersection lines between the fitting planes of rock mass surfaces (Slob et al., 2007; Gigli and Casagli, 2011) and the principle curvature of the vertices on the digital surface model of the rock mass (Umili et al., 2013) respectively. However, these two approaches are both indirect ways to identify fractures from TLS data, and the results rely generally on the data pre-processing. For instance, result of the former approach highly depends on the goodness of fitting planes and segmentation accuracy of the rock mass; whereas that of the latter one is largely influenced by the mesh quality and smooth degree.

In this paper, we proposed a new and simple approach to identify fractures directly and thus acquire surface density from 3-D surface model of natural outcrops generated from TLS data. We take one outcrop from the Shizigou anticline in the Qaidam Basin (NW China) as the case to validate the method and obtain optimal parameters. The results show that the proposed method can detect the fractures well and eliminate most redundant information if suitable parameters are chosen. Though requiring further improvement, the method provides for the first time an unbiased way to identify fractures, so that results from different data sources and interpreters can be well correlated. We believe that it will help a lot in analyzing the development of fractures and other related fields.

## 2. Data collection and pre-processing

Our study is based on TLS data collected from a Riegl VZ-1000 Terrestrial Laser Scanner with highest resolution of 3 mm. It's one of the mostly commonly-used scanner machine, and designed to be easily manipulated in the field. The scanner is equipped with a calibrated Nikon D300 digital camera mounted rigidly on top of the instrument body. Captured digital images are therefore registered to the scanner coordinate, allowing the RGB color to be later assigned onto the 3D geometry (McCaffrey et al., 2005; Hodgetts, 2013).

Selecting appropriate outcrops for study is also of great importance for data collection, and we followed the four rules proposed by Enge et al. (2007) in the selection process: (1) suitability to the problem, (2) easy accessibility, (3) high quality (void of vegetation) and (4) high level of three dimensionality. The sensor must be positioned as orthogonally to the target as possible to gain the best scanning data.

Data pre-processing in this paper contains four steps. The first is the scan registration and interest area selection. A scanning survey usually contains several scan positions (sites) in order to get a complete coverage of the target outcrop (Buckley et al., 2008; Hodgetts, 2013). It is therefore quite important to merge data (called as “registration”) from different sites together, because it affects directly the precision and accuracy of the data for analysis. We usually use artificial tie-points to ensure the veracity of data merging. The second is to clean and decimate vegetation and other obvious redundancies which can be conducted easily in Riegl Pro manually or automatically. The third step is data resampling and export. The point cloud data of the interest region is resampled with a specified precision according to the research requirement, and then exported as any format containing 3-D coordinates (x, y, z values) under Scanner's Own coordinate system (SOCS) whose origin is closely related to the scanning targets (Fig. 1a). Fourthly, a noise reduction algorithm is performed on the exported point cloud data to reduce the noise caused by dust, particle and dynamic disturbances in the open scanning environment (Khoshelham et al., 2011). Eventually, we could obtain a point cloud data which is just the interest region with a little noises.

## 3. Fracture extraction

### 3.1. Triangulation

Triangulation is to link the point cloud via a series of triangles with the aim of producing a solid surface (mesh, triangulated irregular network) that is essential to identify fractures (Buckley et al., 2008; García-Sellés et al., 2011). It is possible and appropriate to form a solid surface from a point cloud data, as a 2-D Delaunay triangulation (Delaunay, 1934) finds the best criteria for triangle creation automatically from projected points (McCullagh, 1998). In contrast, the 3-D Delaunay methods is proved to be unqualified as to generate loads of unexpected surfaces and edges, where points of all directions are connected on 3-D adjacency to form a solid instead of a plane. To solve this problem we follow the procedure proposed by Buckley et al. (2008) and García-Sellés et al. (2011) to generate 2-D mesh from the projected point cloud (Fig. 1).

We firstly project the 3-D points onto a plane. The plane is usually chosen as the one which is perpendicular to the scan direction with angles and distances known relative to the instrument position (xy plane in the SOCS, Fig. 1A and B) because (1) it is normal to and thus reflects most details of the target outcrops, and (2) least points overlap on this plane after projection. The 2-D topological relationship is then generated following the 2-D Delaunay triangulation method (Delaunay, 1934; Fig. 1B). And lastly, the 2-D topological relationship is projected back to form a 3-D mesh according to the different z values of different points, and the topological relationships among different triangles remain unchanged after the transformation (Fig. 1B and C).

### 3.2. Fracture identification

We proposed a new and simple algorithm to identify structural fractures directly from the constructed 3-D mesh. The structural fracture line of natural outcrops generally has sharp edges, and is created by the intersections of different neighboring planes. The algorithm is based on the assumption that structural fractures can be geometrically identified as sharp edges of neighboring planes with large angles. It is therefore reasonable to determine whether a line should be marked as part of a fracture (or fracture segment) by comparing the intersecting angle of the two related surfaces with a threshold angle ($\alpha$). If the angle is larger than $\alpha$, we regard the line as a fracture segment and mark it as red (Fig. 2).

The identified fracture segments following the above algorithm are usually discrete with plenty of noises caused mainly by weathering, rock collapse etc. We put forward three steps to eliminate these noises and obtain as much useful information as possible (Fig. 3). The first step is to get fracture lines by connecting adjacent fracture segments that are within a certain number of mesh segments ($N$) by using breadth first search algorithm (Donald, 1999; Fig. 3A). In practice, $N$ is usually regarded as a constant value between 0 and 4 and we use 2 in this paper (purple circled in Fig. 3A). Through this step, related fracture segments are connected together and named as new fracture line. This makes the identified fracture lines more continuous and helps users to judge whether the fracture lines are real or not.

The second step is to delete the redundancies of fracture lines (as indicated by purple circles in Fig. 3B) by using minimum spanning tree algorithm (Pettie and Ramachandran, 2002). The redundancies mainly refer to the bifurcate fracture segments on a fracture line. Through this step, most furcation on fracture lines are clipped, making the identified fractures more straight.

The third step is to delete the fracture lines containing fewer fracture segments than a specified number ($M$) as marked by purple circles in Fig. 3C. The threshold delete number ($M$) of fracture segments is also regarded as a constant value and specified as 10 in

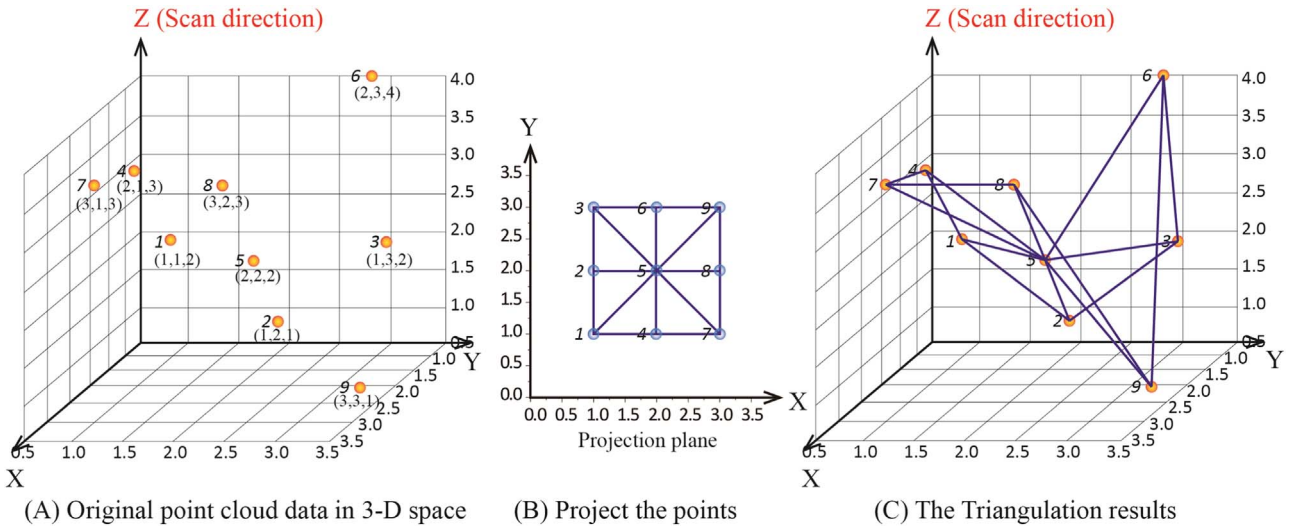


**Fig. 1.** Explanation for the triangulation of point cloud data. We assume Z axis direction as the scan direction so that the x-y plane is the projection plane. The left numbers represent the serial number of each point. A. Display of the point cloud in the 3-D space. B. All the points are projected to the projection plane and 2-D Delaunay triangulation is carried out to get the topological relationship. C. The 2-D topological relationship is projected back to the 3-D point cloud to get a 3-D mesh.

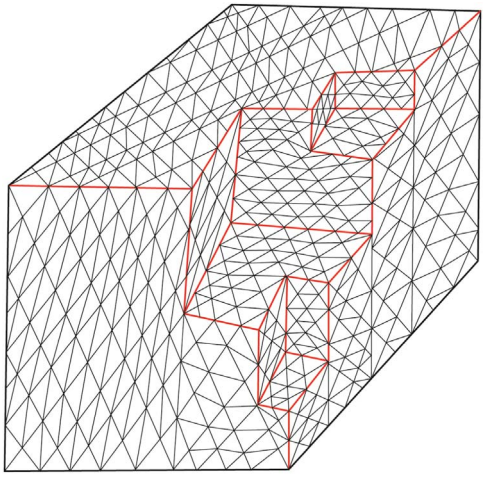

**Fig. 2.** Sketch map showing the mark of fracture identification results on 3-D mesh. The potential segments of mesh are marked in red according to the angle between two adjacent triangle planes.

this paper according to data resolution and research purpose. Through this step, short fracture lines that are not in the research scope or unnecessary are removed, further reducing the unnecessary noises caused by rock collapse and weathering etc.

### 3.3. Surface density acquirement

There are generally three methods to obtain structural fracture density, including line density, surface density and volume density (Dershowitz and Herda, 1992), in which surface density is the best method since it is a good proxy to quantify the development of fractures in a specific area. All the triangle mesh and lines are projected to the projection plane (the xy plane in Fig. 1A) to obtain $\sum L$ and $S$. Then the fracture surface density is calculated using the following formula:

$$f = \frac{\sum L}{S} \quad (1)$$

Where $f$ means the surface density, $\sum L$ represents the sum of projected fracture lengths, $S$ represents the projected area.

## 4. Case studies and calibration of parameters

We now use the TLS data collected in the Shizigou anticline of the western Qaidam Basin (NW China) to validate the proposed method. We also measured the fractures in the field and on the photographs at the same outcrop to calibrate the result and obtain optimal values of the two parameters: the threshold angle ($\alpha$), and the spatial resolution ($R$) of exported data.

### 4.1. Geology background

The Qaidam Basin, with an area of 120,000 km$^2$ and an average elevation of ~3000 m, is the largest petroliferous sedimentary basin inside the Tibetan Plateau, northwest China. It is surrounded by the Altyn Tagh Fault to the northwest, the Qilian Mountain to the northeast and the East Kunlun Mountain to the south (Fig. 4). A number of anticlines and synclines were formed inside the basin due to intense NE-SW-directed crustal shorting in the Late Cenozoic (Zhou et al., 2006; Wu et al., 2014), including the studied NW-trending Shizigou Anticline in the southwest. The Shizigou anticline formed under the control of a NE-dipping thrust, and thus has a steep southwest limb and a nearly flat northeast limb (Fig. 4). The rocks exposed in the Shizigou area are basically late Cenozoic, and composed mainly of non-marine sandstone, siltstone, mud stone and conglomerate. Contacts between these formations are generally conformable. Rocks are well exposed with abundant structural fractures along the valleys crossing the anticline, bare of vegetation and easily reached by vehicles, making itself a suitable place to verify the usability of the method proposed in this paper. There is also a big fractured reservoir for hydrocarbon in tight sandstones in the Shizigou anticline (Xiao et al., 2012; Zang et al., 2012; Wu et al., 2014; Zeng et al., 2012b), which makes the study here more meaningful.

### 4.2. Measurement in the field

Fig. 5 shows the studied outcrop in the core of Shizigou Anticline. The exposed rocks consist mainly of mudstones and sandstones of late Miocene age. We measured the fractures in the field and detected fractures indoors manually on high-resolution images (Fig. 5B), and the calculated surface density is 0.93 m$^{-1}$.

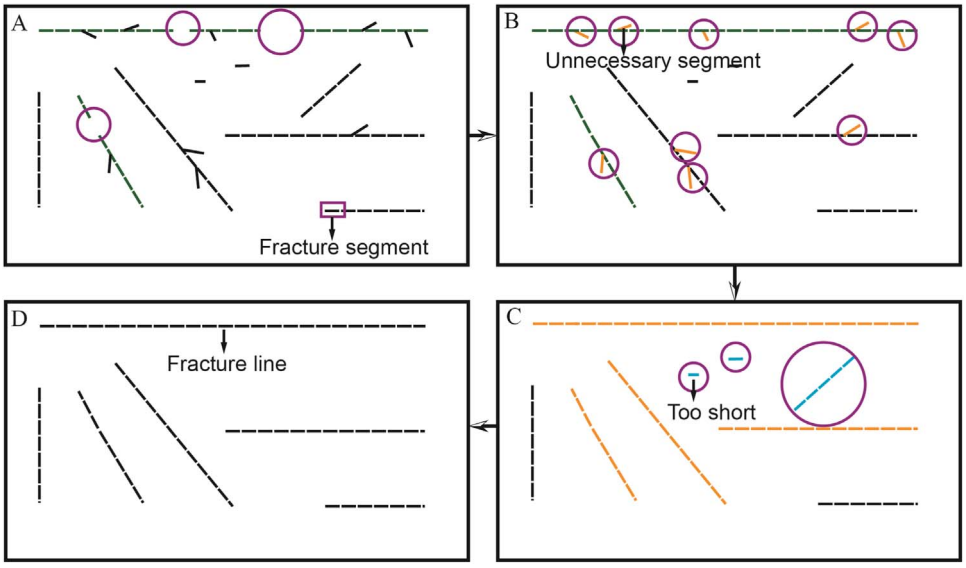


**Fig. 3.** Flow of identifying structural fractures. A. Get the original fracture segments. (The small line segments are used to simulate original fracture segments) B. Connect the small segments circled in A to obtain a fracture line by adding some small segments. C. Delete the unnecessary fracture segments which are circled in B to obtain straight lines. D. Delete the fracture lines containing fewer fracture segments than a specified number which are circled in C.

### *4.3. Fracture identification and calibration of parameters*

We used the Riegl VZ-1000 to scan the outcrops in the research area, and obtained the digital point cloud data of the target outcrop. The above proposed method (Fig. 3) was applied to identify structural fractures, and a quantified surface density number is calculated as a metric to evaluate the two important parameters: threshold angle ($\alpha$) and the resolution ($R$) of exported point cloud data. We try to establish

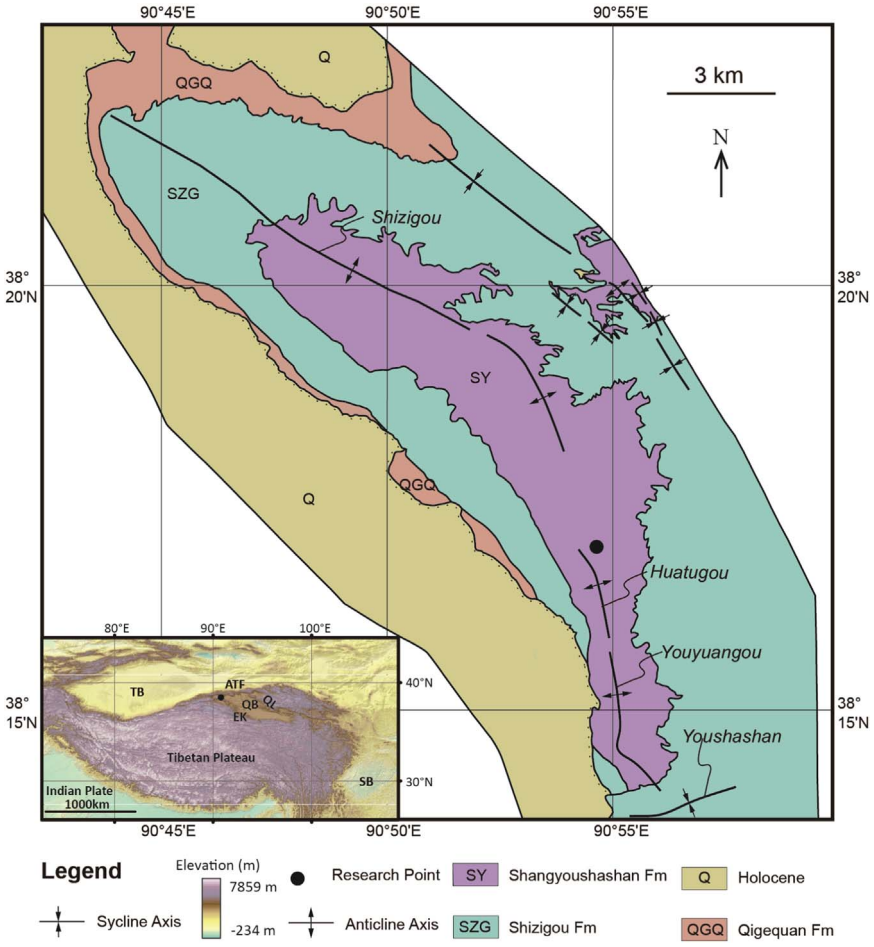


**Fig. 4.** Simplified geological map of the Shizigou Anticline of the western Qaidam Basin with location of the research point shown by the black point. Inset in the left bottom is the DEM map of Tibetan Plateau and adjacent areas, and the black point marks the location of the Shizigou Anticline. ATF=Altyn Tagh Fault, EK=East Kunlun Mountain, QB=Qaidam Basin, QL=Qilian Mountain, TB=Tarim Basin, SB=Sichuan Basin.

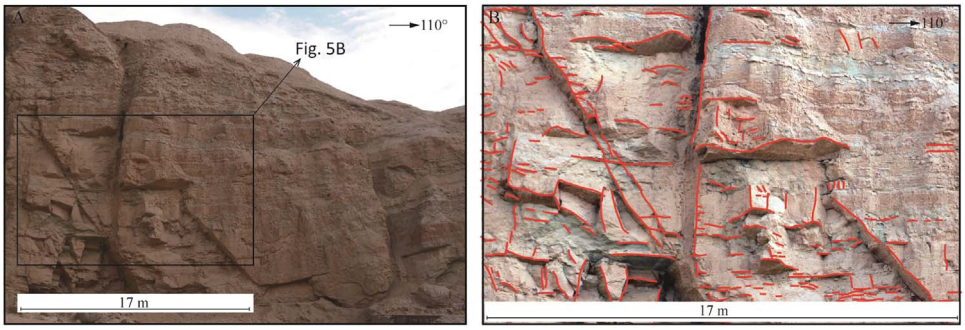


**Fig. 5.** A. Outcrop photos of the research point of this paper, interbedded mudstone and sandstone. B. The result of fracture identification manually on an image with surface density 0.93 $m^{-1}$.

a self-adaptive way to obtain the optimal values of these two parameters, which can provide a method to specify appropriate values of parameters for any case.

We use the data to test most possible values of these two parameters, angle between 30° and 80° with a step of 5° and resolution between 0.01 m and 0.15 m with a step of 0.01 m. The surface density value of each pair of angle and resolution is shown as Fig. 6A. According to the 3-D graph, we can see that the density value decreases with angle and resolution. In addition, we've got the contour map of surface density values influenced by angle and resolution (Fig. 6B), so as to know the density variation trend with angle and resolution. As can be seen from the contour map, surface density decreases with both angle and resolution.

In order to explore the influence of R more clearly, the density variation with resolution (between 0.01 m and 0.15 m with a step of 0.01 m) at three representative angle (35°, 40°, 45°) are extracted individually (Fig. 6C). Meaningfully fracture surface density varies pretty smoothly when the resolution is larger than about 0.1 m, signifying the breakthrough point of resolution and indicating the most prominent part with much less redundancy. 0.1 m is exactly the

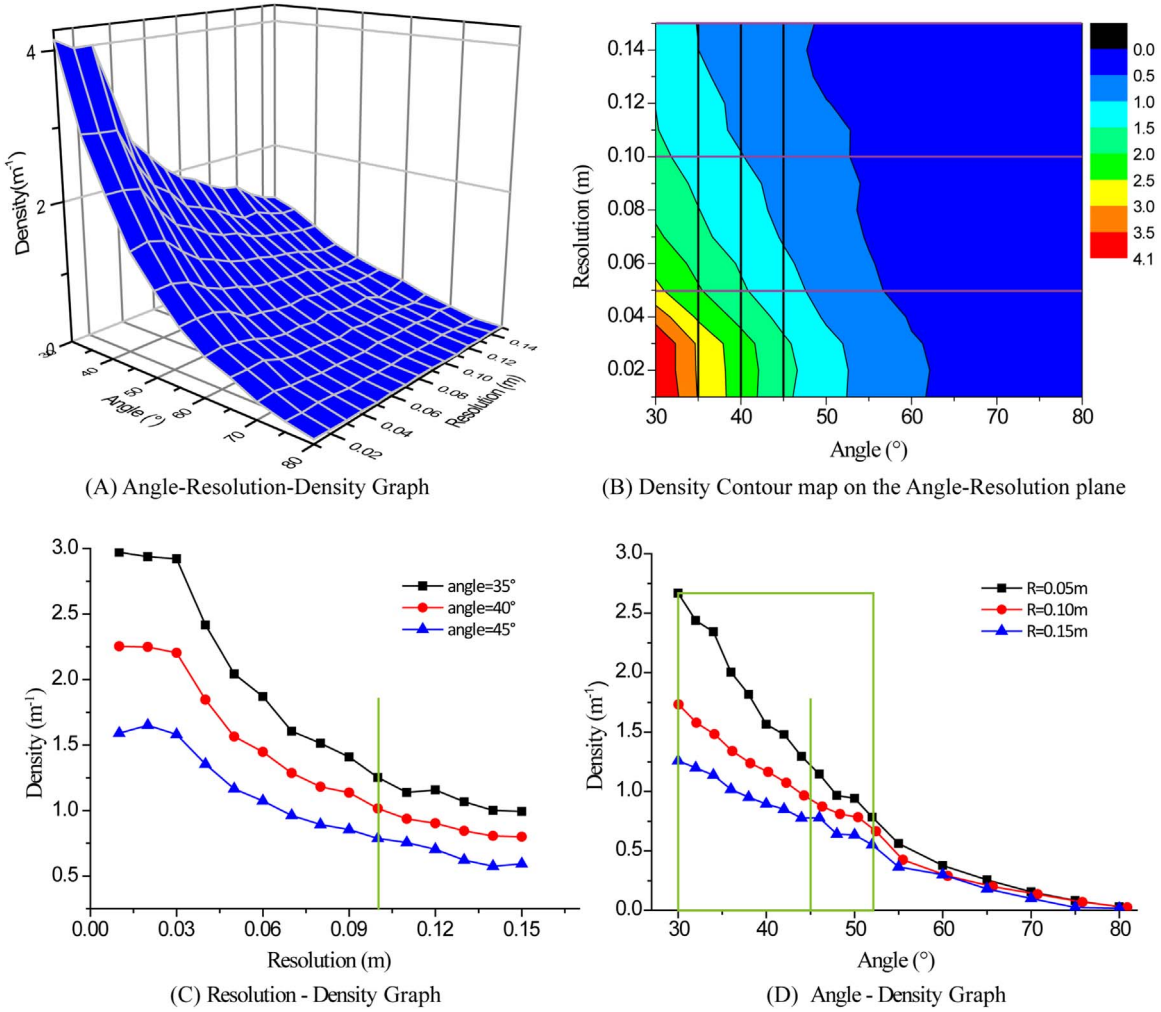


**Fig. 6.** A. The three-dimensional diagram of angle and resolution influence for surface density. B. The contour map of surface density values influenced by angle and resolution. C. Resolution influence diagram at three representative angle (vertical lines in B) to obtain the optimal resolution, here the green line represents the best resolution value 0.10 m. D. Angle influence at three representative resolution (horizontal lines in B) to obtain the optimal angle value, we can obtain better results in the green triangle angle range and the green line suggests 45° as the best angle value.

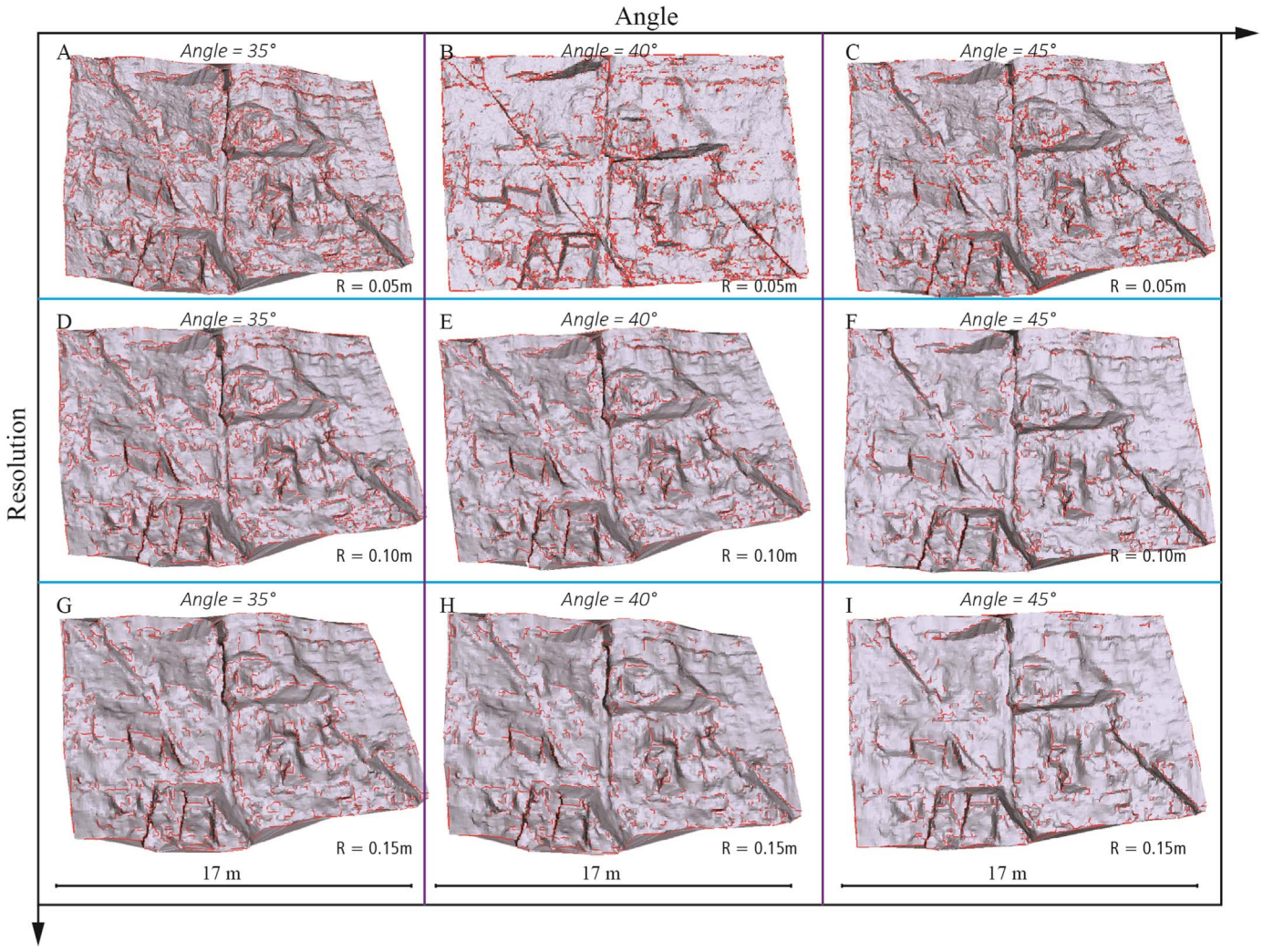


**Fig. 7.** Representative identification results with different angles and resolutions. The horizontal direction displays the angle comparison and the vertical direction displays the resolution comparison for identification results.

shortest fracture line expected to be identified considering the scale of target fractures, therefore the length of the shortest fracture line expected to be identified can be specified as the optimal resolution value. Moreover, the density variation with angle (between 30°and 54° with a step of 2°) at three representative resolution (0.05 m, 0.10 m and 0.15 m) are extracted individually (Fig. 6D) to obtain optimal angle values. From these graphs and the identified results, the identified results are too less when $\alpha$ is bigger than about 55° and the identified results are too complicated when it is smaller than 30°, therefore the results will be more accurate when $\alpha$ is between 30°and 55°. Analyzing the results in the specified angle range, the surface density varies slower when the angle increases to about 45°, suggesting a more stable point which means stable results and less redundancy. Therefore angle of 45° and resolution of 0.1 m are regarded as the most appropriate values to identify fractures with this method for this case.

Representative identification results at different resolutions and angles are shown in Fig. 7. They show that higher resolution (Fig. 7 A, B and C) or smaller angle (Fig. 7A, D and G) results in more redundancies that may be caused by weathering, rock collapse, etc., while lower resolution (Fig. 7G, H and I) or bigger angle (Fig. 7C, F and I) leads to more omission of truly structural fractures. According to fracture scale expected to be identified, the proposed method can accurately identify most of the structural fractures of the data with optimal parameters: α of 45° and R of 0.10 m, under which condition the density value is very close to the value collected from the image (Fig. 5B). Almost 60% of each structural fracture line can be identified with optimal parameters (Fig. 7F) with little redundancies, compared to the real ones marked in the photos (Fig. 5B), including the ones nearly vertical and horizontal. We can conclude from the case that resolution influences the scale and angle influences the type of structural fractures expected to be identified directly in this method. We regard the most appropriate values are: α=45° and R=resolution of the shortest fracture expected to be identified (i.e., it depends on the scientific scope).

## 5. Discussions

The method proposed in this paper can identify structural fractures based on TLS data to evaluate fracture development with many superiorities. Compared to the principle curvature (Umili et al., 2013) method, the detected lines contain more fragmented information which may be small scale fractures. Some structural fractures neglected easily by human operation can be identified within seconds accurately compared to field measurement and image detection. In addition, we can get different types and scales of fractures by confirming different values of threshold resolution and angle, and a quantified surface density value can be obtained to evaluate the development of structural fractures.

The shortcomings of the method can be summarized as follows: (1) the detection results are not straight lines as manual detection because

of the mesh quality and the method itself. Improving the quality of outcrops as much as possible and resampling point cloud data to make larger triangle meshes can solve this problem to some degree. (2) The method can't differentiate bedding from structural fractures which is an inevitable problem in identifying structural fractures, therefore reducing the bedding boundary area in data selection step is one way to avoid this type of disturbance.

## 6. Conclusions

A wide range of fields are now making use of TLS data because of its high precision and accuracy. This paper proposed a simple and unbiased approach to identify fractures directly from 3-D surface model of natural outcrops generated from TLS data. One outcrop of Shizigou Anticline, Qaidam Basin is chosen to validate this method and obtain the optimal parameters, with surface density acquired from the field and image as references. In the case, the proposed method can accurately identify most of the structural fractures with optimal parameters. Moreover, different types and scales of fractures can be identified by confirming different values of threshold resolution and angle to meet different needs.

Because of its convenience, high speed and accuracy with almost no human intervention, and affected by weathering and shadows slightly, this method can provide important supplement data for fracture related research.

## Acknowledgements

The paper is supported by the National Key Scientific and Technological Projects (Grant nos. 2011ZX05009-001 and 2016ZX05003001-003), and the National Key Research and Development Plan Program (Grant no. 2016YFC060100X). The authors would like to thank the open source graphics library visualization tool kit (VTK) company for the use of their algorithm library, Wenyong Weng for helpful advice and Rui Wang for the implementation of some algorithms. We sincerely appreciate the four anonymous reviewers and the editor for their very helpful comments and suggestions, which greatly improve the quality of this paper.

## References

Ahlgren, S., Holmlund, J., 2003. Using 3-D outcrop laserscan for fracture analysis. Am. Assoc. Pet. Geol. Search Discov. Artic., 40099.
Awdal, A., Healy, D., Alsop, G.I., 2016. Fracture patterns and petrophysical properties of carbonates undergoing regional folding: a case study from Kurdistan, N Iraq. Mar. Pet. Geol. 71, 149–167.
Bao, T., Zhao, J., Xu, M., 2015. Step edge detection method for 3D point clouds based on 2D range images. Opt. Int. J. Light Electron Opt. 126, 2706–2710.
Buckley, S.J., Howell, J.A., Enge, H.D., Kurz, T.H., 2008. Terrestrial laser scanning in geology: data acquisition, processing and accuracy considerations. J. Geol. Soc. 165 (3), 625–638.
Buckley, S.J., Howell, J.A., Enge, H.D., Leren, B., Kurz, T.H., 2006. Integration of terrestrial laser scanning, digital photogrammetry and geostatistical methods for high-resolution modelling of geological outcrops. Remote Sens. Spat. Inf. Sci., 36.
Canny, J., 1986. A computational approach to edge detection. Pattern Anal. Mach. Intell. IEEE Trans. 6, 679–698.
Delaunay, B., 1934. Sur la sphere vide. Izv. Akad. Nauk SSSR, Otdelenie Matematicheskii i Estestvennyka Nauk, 7(793-800), 1–2.
Dershowitz, W.S., Herda, H.H., 1992. Interpretation of fracture spacing and intensity. In: Proceedings of the 33th US Symposium on Rock Mechanics (USRMS). American Rock Mechanics Association.
Donald, E.K., 1999. The art of computer programming. Sorting Search. 3, 426–458.
Enge, H.D., Buckley, S.J., Rotevatn, A., Howell, J.A., 2007. From outcrop to reservoir simulation model: workflow and procedures. Geosphere 3 (6), 469.
Feng, J., Cao, J., Hu, K., Peng, X., Chen, Y., Wang, Y., Wang, M., 2013. Dissolution and its impacts on reservoir formation in moderately to deeply buried strata of mixed siliciclastic–carbonate sediments, northwestern Qaidam Basin, northwest China. Mar. Pet. Geol. 39 (1), 124–137.
Ferrero, A.M., Forlani, G., Roncella, R., Voyat, H.I., 2009. Advanced geostructural survey methods applied to rock mass characterization. Rock. Mech. Rock. Eng. 42, 631–665.
Gale, J.F.W., Reed, R.M., Holder, J., 2007. Natural fractures in the Barnett Shale and their importance for hydraulic fracture treatments. AAPG Bull. 91 (4), 603–622.
García-Sellés, D., Falivene, O., Arbués, P., Gratacos, O., Tavani, S., Muñoz, J.A., 2011. Supervised identification and reconstruction of near-planar geological surfaces from terrestrial laser scanning. Comput. Geosci. 37 (10), 1584–1594.
Gigli, G., Casagli, N., 2011. Semi-automatic extraction of rock mass structural data from high resolution LIDAR point clouds. Int. J. Rock. Mech. Min. Sci. 48, 187–198.
Goodwin, N.R., Armston, J., Stiller, I., Muir, J., 2016. Assessing the repeatability of terrestrial laser scanning for monitoring gully topography: a case study from Aratula, Queensland, Australia. Geomorphology 262, 24–36.
Hart, B.S., 2006. Seismic expression of fracture-swarm sweet spots, Upper Cretaceous tight-gas reservoirs, San Juan Basin. AAPG Bull. 90, 1519–1534.
Hodgetts, D., 2013. Laser scanning and digital outcrop geology in the petroleum industry: a review. Mar. Pet. Geol. 46, 335–354.
Khoshelham, K., Altundag, D., Ngan-Tillard, D., Menenti, M., 2011. Influence of range measurement noise on roughness characterization of rock surfaces using terrestrial laser scanning. Int. J. Rock. Mech. Min. Sci. 48, 1215–1223.
Kuo, C., Brierley, G., Chang, Y., 2015. Monitoring channel responses to flood events of low to moderate magnitudes in a bedrock-dominated river using morphological budgeting by terrestrial laser scanning. Geomorphology 235, 1–14.
Lacazette, A., 2009. Paleostress analysis from image logs using pinnate joints as slip indicators. AAPG Bull. 93, 1489–1501.
Li, Y., Wang, T., 2001. Middle to deep fractural oil reservoir in Shizigou area, Qaidam Basin. Pet. Explor. Dev. 28, 12–15.
Liang, X., Kankare, V., Hyyppä, J., Wang, Y., Kukko, A., Haggrén, H., Yu, X., Kaartinen, H., Jaakkola, A., Guan, F., Holopainen, M., Vastaranta, M., 2016. Terrestrial laser scanning in forest inventories. ISPRS J. Photogramm. Remote Sens. 115, 63–77.
Lohr, T., Krawczyk, C.M., Tanner, D.C., Samiee, R., Endres, H., Thierer, P.O., Oncken, O., Trappe, H., Bachmann, R., Kukla, P.A., 2008. Prediction of subseismic faults and fractures: integration of three-dimensional seismic data, three-dimensional retrodeformation, and well data on an example of deformation around an inverted fault. AAPG Bull. 92 (4), 473–485.
Lopez-Molina, C., De Baets, B., Bustince, H., Sanz, J., Barrenechea, E., 2013. Multiscale edge detection based on Gaussian smoothing and edge tracking. Knowl. Based Syst. 44, 101–111.
Masaferro, J.L., Bulnes, M., Poblet, J., Casson, N., 2003. Kinematic evolution and fracture prediction of the Valle Morado structure inferred from 3-D seismic data, Salta province, northwest Argentina. AAPG Bull. 87, 1083–1104.
McCaffrey, K., Jones, R.R., Holdsworth, R.E., Wilson, R.W., Clegg, P., Imber, J., Holliman, N., Trinks, I., 2005. Unlocking the spatial dimension: digital technologies and the future of geoscience fieldwork. J. Geol. Soc. 162 (6), 927–938.
McCullagh, M.J., 1998. Quality, use and visualisation in terrain modelling. In: Lane, S.N., Richards, K.S., Chandler, J.H. (Eds.), Landform Monitoring, Modelling and Analysis. Wiley, Chichester, 95–117.
Olson, J.E., Laubach, S.E., Lander, R.H., 2009. Natural fracture characterization in tight gas sandstones: integrating mechanics and diagenesis. AAPG Bull. 93 (11), 1535–1549.
Ouédraogo, M.M., Degré, A., Debouche, C., Lisein, J., 2014. The evaluation of unmanned aerial system-based photogrammetry and terrestrial laser scanning to generate DEMs of agricultural watersheds. Geomorphology 214, 339–355.
Pettie, S., Ramachandran, V., 2002. An optimal minimum spanning tree algorithm. J. ACM (JACM) 49 (1), 16–34.
Prioul, R., Jocker, J., 2009. Fracture characterization at multiple scales using borehole images, sonic logs, and walkaround vertical seismic profile. AAPG Bull. 93 (11), 1503–1516.
Slob, S., Hack, R., Turner, A.K., 2002. An approach to automate discontinuity measurements of rock faces using laser scanning techniques. In: ISRM International Symposium-EUROCK 2002. International Society for Rock Mechanics.
Slob, S., Hack, H., Feng, Q., Röshoff, K., Turner, A.K., 2007. Fracture mapping using 3D laser scanning techniques. In: Proceedings of the 11th Congress of the International Society for Rock Mechanics, Lisbon, Portugal, 1*1., pp. 299–302.
Strijker, G., Beekman, F., Bertotti, G., Luthi, S.M., 2013. FEM analysis of deformation localization mechanisms in a 3-D fractured medium under rotating compressive stress orientations. Tectonophysics 593, 95–110.
Sturzenegger, M., Stead, D., 2009. Close-range terrestrial digital photogrammetry and terrestrial laser scanning for discontinuity characterization on rock cuts. Eng. Geol. 106, 163–182.
Su, N., Zou, L., Shen, X., Guo, F., Ren, Y., Xie, Y., Li, J., Wu, J., 2014. Fracture patterns in successive folding in the western Sichuan basin, China. J. Asian Earth Sci. 81, 65–76.
Sun, Q., Hou, Y., Tan, Q., 2016. A subpixel edge detection method based on an arctangent edge model. Opt. Int. J. Light Electron Opt. 127, 5702–5710.
Umili, G., Ferrero, A., Einstein, H.H., 2013. A new method for automatic discontinuity traces sampling on rock mass 3D model. Comput. Geosci. 51, 182–192.
Wang, W., Zhao, W., Huang, L., Vimarlund, V., Wang, Z., 2014. Applications of terrestrial laser scanning for tunnels: a review. J. Traffic Transp. Eng. 1, 325–337.
Watkins, H., Butler, R.W.H., Bond, C.E., Healy, D., 2015. Influence of structural position on fracture networks in the Torridon Group, Achnashellach fold and thrust belt, NW Scotland. J. Struct. Geol. 74, 64–80.
Wu, L., Xiao, A., Ma, D., Li, H., Xu, B., Shen, Y., Mao, L., 2014. Cenozoic fault systems in southwest Qaidam Basin, northeastern Tibetan Plateau: geometry, temporal development, and significance for hydrocarbon accumulation. AAPG Bull. 98 (6), 1213–1234.
Xiao, F., Bao, J., Zhu, G., Zhang, W., He, H., 2012. Comparison of the geochemical characteristics of crude oils from typical oilfields in Western Qaidam Basin. J. Earth Sci. Environ. 34 (4), 43–52.
Zang, S., Cui, J., Zheng, Y., Xu, W., Wei, J., 2012. Analysis of characteristics of low-permeable reservoir with micro-fracture and their origins of the Neogene Youshashan formation in Nanyishan oilfield, Qaidam Basin. J. Palaeogeogr. 14 (1),

133–141.
Zeng, L., Tang, X., Wang, T., Gong, L., 2012b. The influence of fracture cements in tight Paleogene saline lacustrine carbonate reservoirs, western Qaidam Basin, northwest China. AAPG Bull. 96 (11), 2003–2017.
Zeng, L., Tang, X., Qi, J., Gong, L., Yu, F., Wang, T., 2012a. Insight into the Cenozoic tectonic evolution of the Qaidam Basin, Northwest China from fracture information. Int. J. Earth Sci. 101 (8), 2183–2191.
Zhou, J., Xu, F., Wang, T., Cao, A., Yin, C., 2006. Cenozoic deformation history of the Qaidam Basin, NW China: results from cross-section restoration and implications for Qinghai-Tibet Plateau tectonics. Earth Planet. Sci. Lett. 243 (1–2), 195–210.